Journal of the Taiwan Institute of Chemical Engineers 154 (2024) 105083

Contents lists available at ScienceDirect

Journal of the Taiwan Institute of Chemical Engineers

journal homepage: www.journals.elsevier.com/journal-of-the-taiwan-institute-of-chemical-engineers

An impact of sea sponge-derived hard carbon with the symbiosis of sodium ion battery and biomedical applications

T. Meenatchi [a], R. Subadevi [a,*], P. Kumar [b], S. Raghu [c], Wei-Ren Liu [d,*], M. Sivakumar [a,*]

[a] #120, Energy Materials Lab, Department of Physics, Science Block, Alagappa University, Karaikudi 630 003, Tamil Nadu, India
[b] Department of Animal Health and Management, Science Block, Alagappa University, Karaikudi 630 003, Tamil Nadu, India
[c] Department of Chemistry, Vel's University, Chennai 600 025, Tamil Nadu, India
[d] Department of Chemical Engineering, R&D Center for Membrane Technology, Research Center for Circular Economy, Chung-Yuan Christian University, Chung-Li 32023, Taiwan, ROC

ARTICLE INFO

Keywords:
Sea sponge
Pyrolysis
Activating agent
Mesoporous structure
Sodium-ion batteries
Biomedical applications

ABSTRACT

Background: Sodium is pervasive and enormous compared to that of lithium. SIBs have turned out to be factual competitors to LIBs besides storage purposes, the power battery technology intended for electric vehicle transport. The choice of selecting SIBs is effective due to their alluring properties of biomaterials for synthesizing electrode materials. Hard carbon, (HC) owing to its amorphous and highly porous nature of the material leads to the intercalation/deintercalation of sodium ions.

Methods: In this work, the sea sponge (SS) was carbonized by the chemical-activating pyrolysis method. The as-prepared HCs using different chemical activating agents (KOH, NaOH, $ZnCl_2$) reveals the diversified sodium-ion storage behaviors.

Significant findings: SS attained a charge capacity of 347.39 mAh g^{-1} at a 0.1 C rate. The half maximal (IC_{50}) of sea sponge-derived hard carbon was found to be 11.5, 11.4, 10.7 μg/mL against breast cancer cells (MDA MB - 231). The present work communally addressed the potential anode material and effective cancerous activity of sea sponge-derived hard carbon material.

1. Introduction

The usage of energy spans a very large part of our daily routine. The forthcoming era of lacking energy storage devices becomes very threatening for everyone on earth and it will be more difficult if it is not encountered at the earliest. Even, the lithium-ion batteries placate the energy scarceness, still, it is vital to pursue an alternative resource. In these recent years, for powering a range of devices from cellphones to electric vehicles, the cost of lithium rose from $383 to $929 million [1,2,3]. Thereupon, it is decisive to look for a better substitute for battery technology owing to the inadequate lithium reserve. Sodium-ion batteries with a standardized mechanism to that of LIBs and undoubtedly lower cost are emerging as a justifiable solution for large-scale commercialization. Selecting appropriate anode materials with virtuous EC performance for SIBs is escalating rapidly in the battery community. Condescending cycling performance can be obtained by espousing anodes, that exhibit low-volume expansion through intercalation/deintercalation of sodium ions. There has been a surfeit of aspirants for sodium ion battery anodes. Graphite serves as an anode for LIBs, which does not deliver a meaningful capacity in SIBs. Subsequently, several sorts of anode materials transition metal oxides, alloying type materials, conversion materials, phosphorous and carbon materials have been studied [4–10]. Nonetheless, barriers such as structure instability, high discharge potential, low reversible capacity, and low initial coulombic efficiency still exist. Though, huge volume expansion and lack of reversibility restrict their usage, as commercially stable anode materials. These shortfalls can be fixed by adopting hard carbon (HC) owing to the least production costs and environmental friendliness [11].

Hard carbon, (HC) owing to its amorphous and highly porous nature of the material leads to the intercalation/deintercalation of sodium ions. So far, incredible efforts have been ardent to enhance HCs sodium storage capacity, wherever the effects of the distinctiveness of carbon precursors, and structure have been analyzed. HC is non-graphitizable

* Corresponding authors.
E-mail addresses: subadevir@alagappauniversity.ac.in (R. Subadevi), WRLiu1203@cycu.edu.tw (W.-R. Liu), sivakumarm@alagappauniversity.ac.in (M. Sivakumar).

https://doi.org/10.1016/j.jtice.2023.105083
Received 9 March 2023; Received in revised form 23 June 2023; Accepted 10 August 2023
Available online 27 August 2023

and a fundamental understanding of its structure, ion-transfer process, storage mechanism, and electrolytic interface is indispensable for improving the performance of HC. For emerging economically cost-effective HC anode for SIBs, numerous biomass sources such as banana peels [12], coconut sheath [13], pomelo peels [14], orange peel [15], silk [16], sucrose [17] have been utilized as base materials. This biomass-derived carbon can be demonstrated for its justifiable performance as an anode for SIBs. Consequently, there are yet two solutions to simplify the commercialized process of biomass-based HCs. They are (i) widening the carbonization technique that leads to good performance and yields more product after several biomass sources with the lowermost energy consumption and (ii) an inclusive perception of sodium-ion storage deeds of various biomass-based HCs. Eventually, HC is uneven, curved, and disordered and mostly comprises of single-layered carbon atoms that are arbitrarily and closely linked. The most commonly used chemical activating agents for enhancing the porous nature of the HC material are KOH, NaOH, H_3PO_4, and $ZnCl_2$ [18,19]. Generally, the activating agents are used to activate the materials and to enhance their properties for application and fabrication purposes. In this regard, the HC material requires high pore diameter, for the charge transfer process and a highly disordered structure. The activating agents used here are NaOH, KOH, and $ZnCl_2$.

Thus, organic compounds can be adopted due to their low cost of production, and environmental benignity. In these aspects, the organic compounds have various advantages including their tunable redox property, chemical diversity, less weight, automatic flexibility, and cost-effectiveness that offers extensive selection of applications for the usage in batteries. Sea-sponge (Phylum Porifera) are again and again overlooked as a significant component of underneath marine ecologies. They are known to execute numerous purposeful roles, particularly as reef-building organisms in both the shallow and deep sea [20,21]. It supports areas of high biodiversity and acts as a hotbed for several fish species. It influences the chief production by regulating nutrient obtainability. This ecological importance is flattered by their fiscal potential from ergonomics and innovative chemicals for pharmacological applications.

In this work, the biomass-derived hard carbon is obtained by using sea sponge as a precursor. This work notably increases the performance of energy storage devices. Basically, marine sponges can be considered as a drug treasure house due to their excellent pharmacological properties [22]. In addition, the bioactive terpenes, sterols, fatty acids, alkaloids, cyclic peptides, peroxides, and amino acid derivatives have been described from sponges, which have a high potential to act as an antiviral, anti-protozoal, anti-inflammatory, and anti-fouling activity [23]. Particularly, the utilization of sea sponge-derived hard carbon electrode material acquired by the chemical activating pyrolysis process as a natural precursor has not been addressed in the literature for sodium-ion battery and bio-medical applications. Hence, this work significantly utilizes the sea sponge as a precursor for synthesizing the hard carbon material for sodium-ion batteries and anti-cancer activity. In most of the reports, the pyrolyzing temperature has widely been inspected, but activating agents – a crucial key factor has been always ignored. In this work, the as-prepared HCs using different chemical activating agents (KOH, NaOH, $ZnCl_2$) reveals the diversified sodium-ion storage behaviors. Basically, sodium-ion batteries require high pore volume and highly disordered structure for the ion transfer process. This work designates the significance of activating agents leading to the large pore diameter in the as-prepared sample. The mechanisms behind the activating agent are as given hereunder:

i. The impact of KOH activation is due to the occurrence of oxygen in the activating agent that affects the steadiness and cross-linking of HC materials. During the activation process, the potassium (K) ion enters the carbon material and disturbs the crystallite arrangement. After pyrolysis, the K salts were removed by washing them several times.
ii. The impression of NaOH activation is owing to the strong corrosive nature of NaOH at high temperatures. This affects the active sites in the char and is etched during the activation process. This results in sequential stimulation reactions with NaOH to form the porous morphological structure.
iii. The influence of $ZnCl_2$ is due to the dehydrating property of $ZnCl_2$. This results in aromatization and charring which leads to a high yield of carbon with a porous structure [13,19].

2. Materials and methods

Sea sponge specimens were collected from the area of Thondi, South Tamil Nadu, India. The sponges were conscientiously washed with deionized water and dried. The obtained material was pre-carbonized at 500 °C. Then it was crushed and activated using various activating agents (KOH, NaOH, $ZnCl_2$). The crushed sample was dipped into the activating agents for 24 h. Then it was eventually centrifuged and desiccated at 110 °C for a day. The obtained sample was pyrolyzed at 900 °C and named K-SS, Na-SS, and Zn-SS.

The interlayer spacing of K-SS, Na-SS, and Zn-SS can be calculated by using the Bragg's equation.

$$n\lambda = 2d\sin\theta \tag{1}$$

$$d = \frac{n\lambda}{2\sin\theta} \tag{2}$$

where λ is the X-ray wavelength, d is the spacing of the diffracting planes, and θ is the angle between the incident rays and the diffracting planes, otherwise known as the Bragg angle.

2.1. Material characterizations

The surface area and porous nature of the sample were characterized using Nova station A at 77 K. The structural morphology of the prepared samples was analyzed by Fourier electron scanning electron microscope (Quanta FEG 250) and Transmission electron microscope JEOL Japan. The X-ray diffraction (XRD) analysis was executed by PAN analytical, X'-pert pro model. Raman spectra was carried out by STR RAMAN, SEKI Corporation (Japan) to identify and confirm the occurrence of carbon phases in the synthesized samples.

2.2. Electrochemical analysis

A slurry of about 80% SS sample 10% carbon black (Super-P) and 10% Polyvinylidene fluoride (PVdF) was mixed in N-methyl pyrrolidone (NMP) as solvent was coated on an Aluminum foil and dried overnight in an oven at 110 °C. The obtained electrode, glass fiber separator, 1 M $NaClO_4$ in ethylene carbonate (EC) and diethylene carbonate (DEC), and Na metal as counter electrode were assembled into a CR-2032 type coin cell in a glove box. The cyclic voltammetry (CV) and charge and discharge (GCD) measurements and electrochemical impedance spectroscopy (EIS) were carried out using a biologic (BCS-815, France) battery tester between 0.01 and 2.8 V vs. Na/Na+ cell couple. Here all the battery performances were examined in an ambient temperature.

2.3. Biomedical activity

2.3.1. MTT assay

Normal (HEK-293) and cancerous (MDA-MB-321) cells used in this study were obtained from the National centre for Cell Science and cultured in accordance with the procedure. The MTT assay is performed to determine the cell viability of SS, K-SS, Na-SS, and Zn-SS as described by Mosmann [24]. The induction of apoptosis was also confirmed by fluorescence microscopy employing fluorescent probes named acridine orange/ethidium bromide (for dual staining) and Hoechst 33,344 (for nuclear staining) [25].

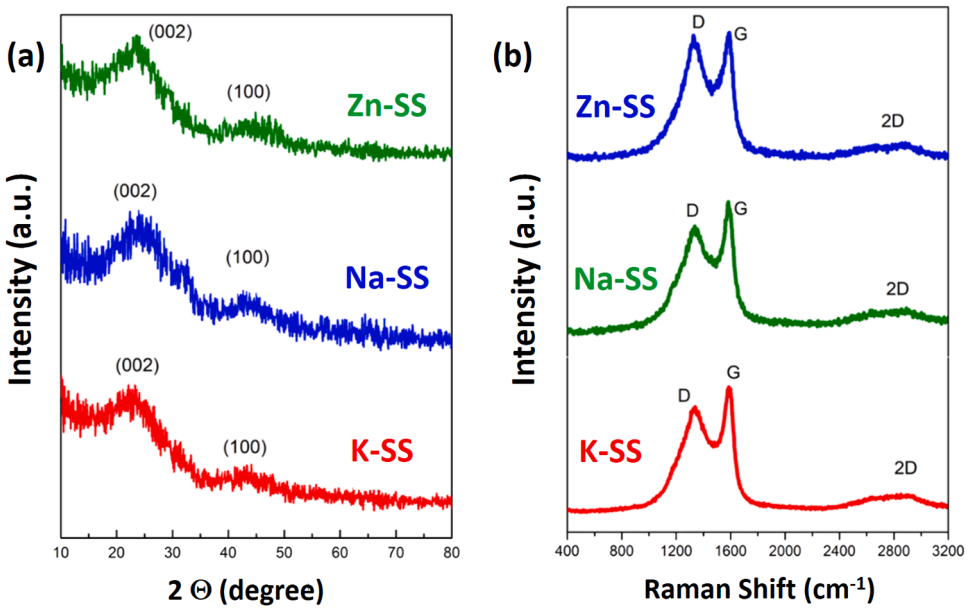

Fig. 1. (a) XRD patterns and (b) Raman spectra of K-SS, Na-SS and Zn-SS samples.

Table 1
Textural properties of SS samples.

No.	Samples	Surface area (m^2/g)	Pore size (nm)	Pore volume (cc/g)
1	K-SS	104.010	3.483	0.002
2	Na-SS	23.356	3.519	0.006
3	Zn-SS	4.295	3.742	0.015

3. Results and discussion

Figure 1(a) shows the XRD patterns of K-SS, Na-SS, and Zn-SS. The peaks at 2θ = 23° and 43° correspond to the (002) and (100) diffraction planes. The peaks with broad shapes confirm the disordered structure of the SS samples. The SS samples at 500 °C activation, do not substantially improve the graphitic disordered structure. At 500 °C the prepared sample is pre-carbonized i.e.) initial stage of carbonization. The TGA-DTA graph was shown in Fig.S1. The TGA graph shows that even after 500 °C, there are some weight losses occur in the raw SS sample. The graph shows the raw materials thermal stability. The pyrolyzing temperature was fixed using thermogravimetric analysis. Basically, in chemical activation process, the material is activated using various activating agents, and were finally pyrolyzed at 900 °C to obtain the carbon materials. (K-SS, Na-SS, Zn-SS). The upshot of the XRD results accompanying the outcome of Raman and BET were shown in the table. Table 1 bespeaks the interlayer spacing (d_{002}) moderately changes while varying the activating agents. The pyrolyzing temperature was fixed using thermogravimetric analysis. From this XRD analysis the interlayer spacing was calculated as 0.37,0.38 and 0.39 nm. This enlarged interlayer spacing may enable the way for Na ions all through the intercalation/ deintercalation process.

Figure 1(b) shows the Raman spectroscopic analysis of K-SS, Na-SS, and Zn-SS. In Raman analysis, the peaks appearing at 1332, 1335, and 1359 cm^{-1} affirm the D band, and 1597, 1582, and 1574 cm^{-1} represent the G band respectively. Generally, the G band is a distinctive characteristic of the graphitic layers which agrees with the carbon atoms' tangential vibration, and the D band resembles the defective structures or disordered carbon. The intensity ratio is used to determine the degree of disorders. The calculated I_D /I_G ratio for the K-SS, Na-SS, and Zn-SS are 0.834, 0.84, and 0.863. The I_D /I_G ratio never goes above 1, which specifies a low degree of disordered nature [26,27,28].

The (FE-SEM) scanning electron microscope in Fig. 2, reveals the effect of the activating agent on the structural morphology of the synthesized HC material (K-SS, Na-SS, ZN-SS). It is clearly shown that the SS-derived HC material has transformed into microspheres by the influence of activating agents. The K-SS, Na-SS, and Zn-SS hard carbon material shows the porous morphology of the material replicating the surface morphology of the natural sea sponges. The surface morphology of the obtained HC materials is a prime factor for electrochemical performance when used as an electrode anode material in NIBs. The activation agents are used here to improve the pore structure of SSHC. After activation, the disordered and uneven morphologies were observed in the images. The as-prepared K-SS, Na-SS and Zn-SS shows the irregular and disordered porous structure. The SEM image of Zn-SS shows more porous structure when compared to K-SS, and Na-SS. This is due to the

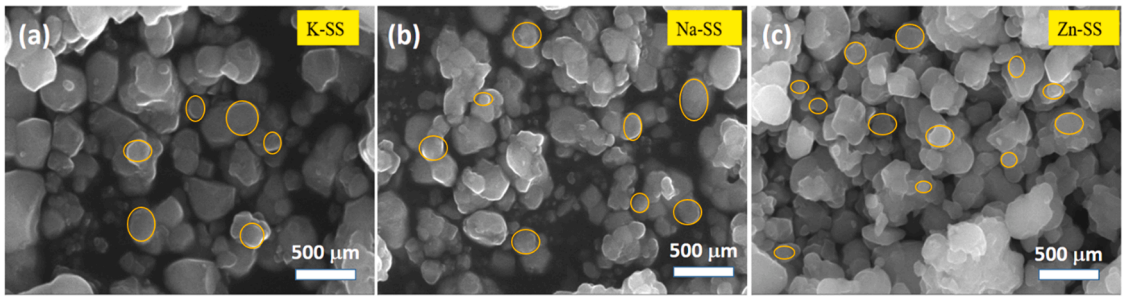

Fig. 2. FE-SEM images of (a) K-SS, (b) Na-SS, and (c)Zn-SS.

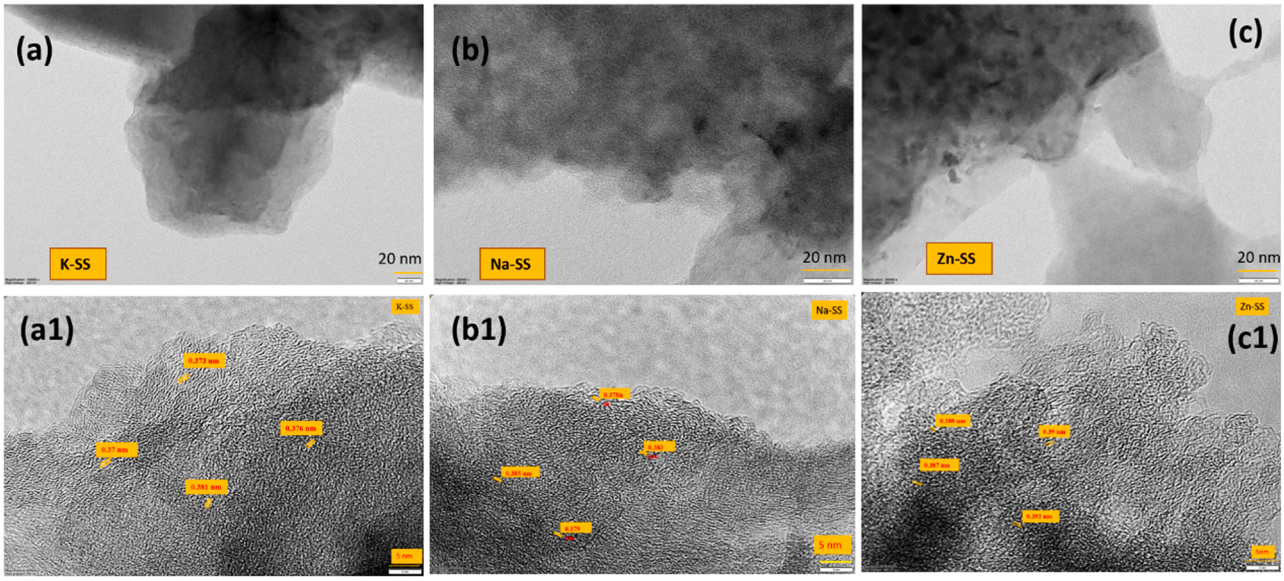

Fig. 3. TEM images of (a, a1) K-SS, (b, b1) Na-SS, and (c, c1) Zn-SS.

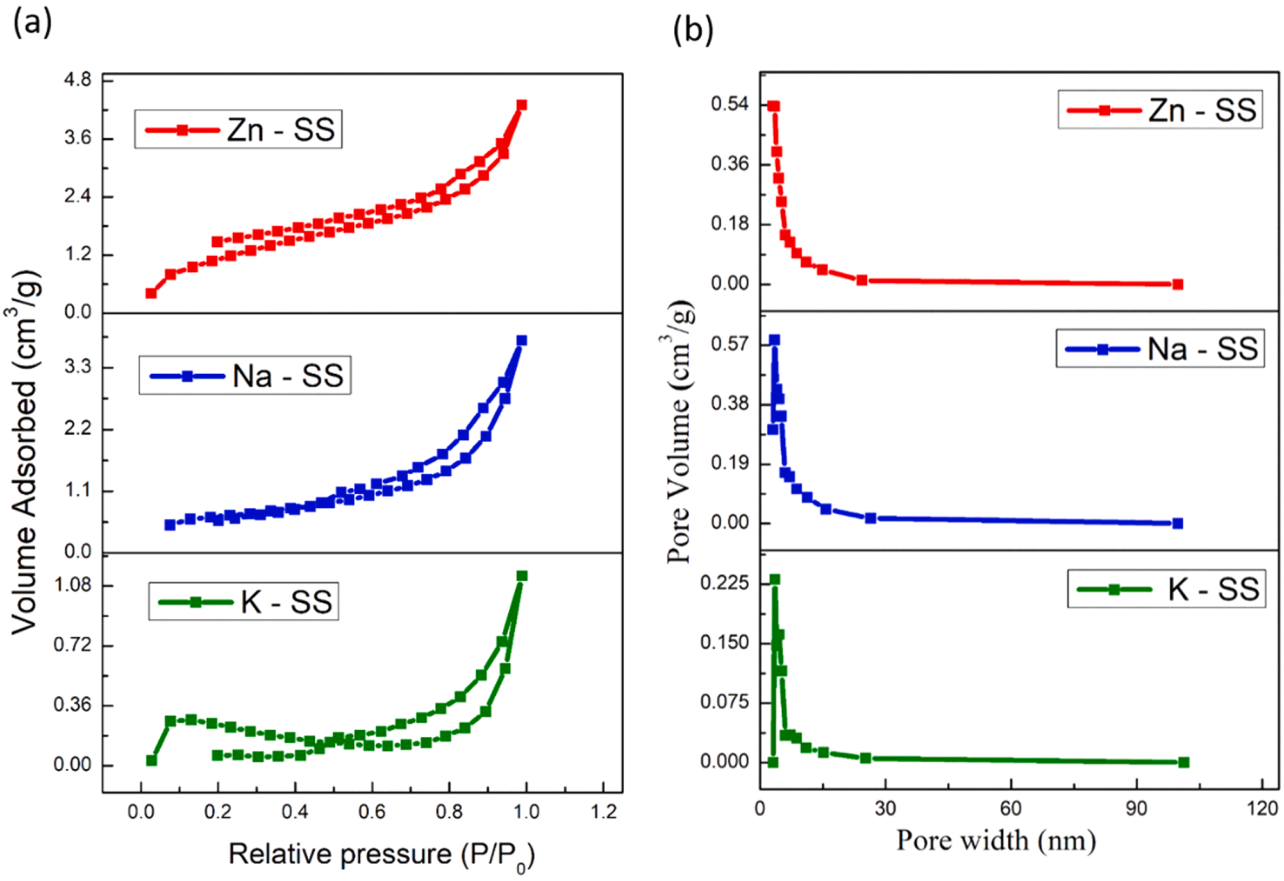

Fig. 4. (a) N_2 adsorption/desorption analysis and (b) Pore size distribution of K-SS, Na-SS, Zn-SS.

effect of activating agents and finer connectivity between the synthesized HC material and electrolyte. The appearance of these spheres can be advantageous for superior electrochemical performances. The mechanism behind these activating agents is explained above.

To analyze the local structure of the SS-derived hard carbon samples, TEM imaging was performed in Fig. 3. Fig. 3 reveals that the prepared carbon materials contain small nano crystallite domains composed of randomly oriented curved graphene layers. This insists that the pyrolysis process using various activating agents yields distinctive hard carbon materials. The structure of the prepared materials may be tuned by annealing temperature and the activating agents used. The disordered arrangement of the carbon leaves a large number of voids in the structure. From this TEM images, it is observed that the interlayer distance of K-SS, Na-SS, and Zn-SS samples is ~0.373, 0.384, and 0.392 nm, which

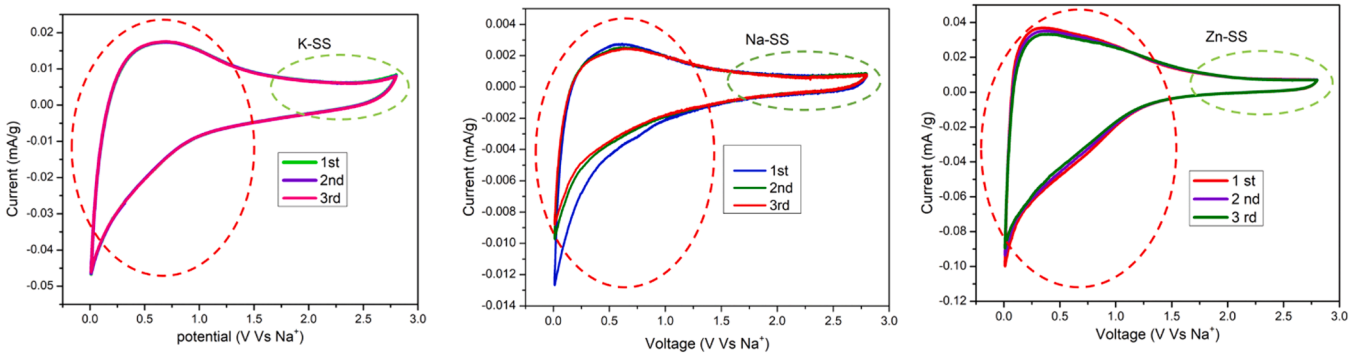

Fig. 5. Cyclic voltammetry of K-SS, Na-SS, Zn-SS.

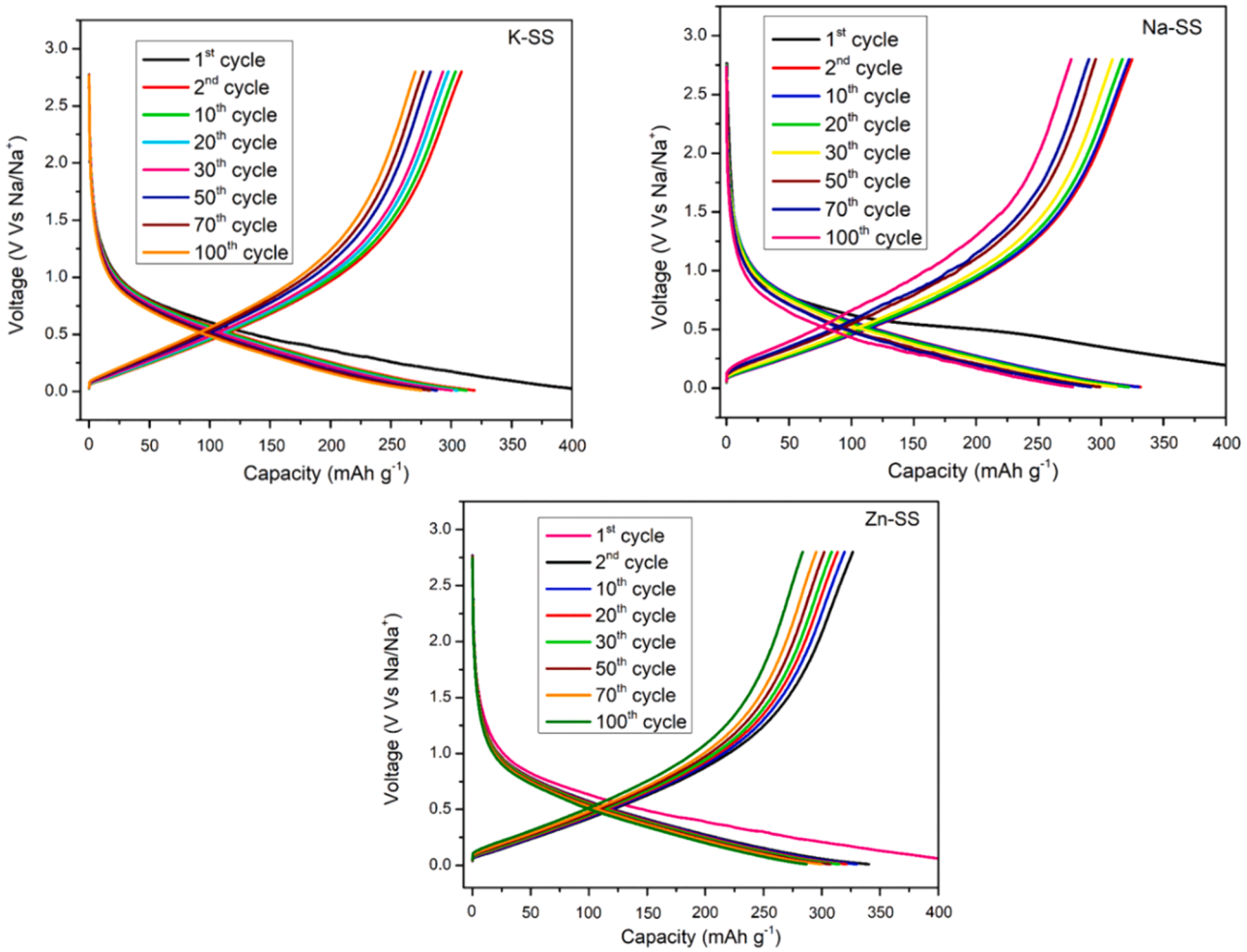

Fig. 6. Galvanostatic charge/discharge profiles of K-SS, Na-SS, Zn-SS.

is higher than 0.335 nm of graphite. It is well in agreement with the XRD analysis. In addition, augmented spacing is preferred for Na storage [29] (Fig. 1).

To explore the porosity and surface area of the hard carbon materials, the pore size distribution and N_2 adsorption/ desorption graphs are shown in Figs. 4 and 5. All the prepared carbon samples evince type IV isotherms correlated with capillary condensation, which is taking place in mesopores, at high pressures. The hysteresis loop (H_3) is in the range between 0.5 and 1.0, indicating that both mesopores & macropores exist in the as-prepared carbons [30]. The pore size distribution further confirms the presence of mesopores in the prepared hard carbon materials. (i.e., K-SS, Na-SS, Zn-SS). The type IV isotherms associated with H_3 loops are often affiliated with slit-like pores in plate-like particles [31]. Moreover, all the prepared SS hard carbon materials reveal a homogeneous behavior over pore size distributions. The surface area of the samples was evaluated as 104.010, 23.356, and 4.295 m^2/g respectively. The volume of the pore and the size of the pore of the synthesized sample increase by varying the activating agents and the carbonization temperature used. It designates that the temperature and activating agents may play a massive impact on the porosity of the carbon. Initially, the raw sea sponge was dried, crushed and turned brown in color. But, after pyrolyzing, the precursor is changed into black

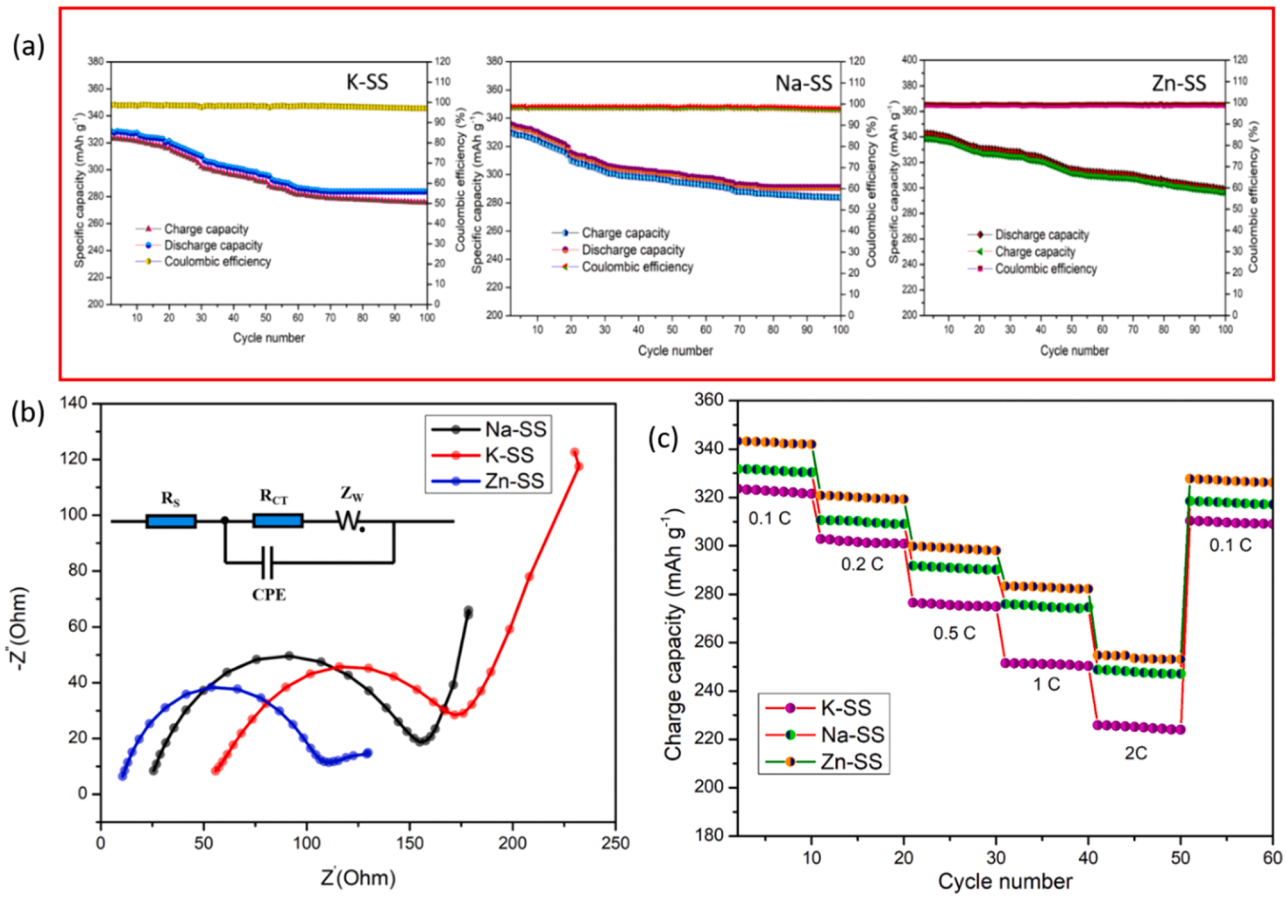

Fig. 7. (a) Coulombic efficiency (b) Nyquist plot for K-SS, Na-SS, Zn-SS (c) Rate capability.

color. This implies that the pyrolyzed temperature also plays an effective impact in the chemical activation pyrolysis process [32]. These observed results are well in accordance with SEM and TEM results.

To scrutinize the influence of activating agents on the electrochemical properties of sea sponge-derived hard carbon materials, cyclic voltammetry (CV) test was carried out. We employ a half cell with sodium (Na) as a counter electrode in the range of potential between 0.01 and 2.8 V at a scan rate of 0.1 Mv s^{-1}. The CV curves of K-SS, Na-SS, and Zn-SS consist of a pair of reduction and oxidation peaks at 0.38 and 0.53 V, 0.37 and 0.47 V, 0.62 and 0.33 V, in accordance with Na intercalation/deintercalation, which is well associated with the literature [11]. The redox peaks at about 0.37 V due to the irreversible reactions of sodium with the functional groups present on the surface of the materials. Then the peaks near 0 V are owing to the Na adsorption on both sides of the walls or sheets of nanopores. The green dotted line indicates the reaction of pseudocapacitive behavior where fast and reproducible Na deposition at pores are taken place. While the red dotted line indicates the residual peaks of redox reactions, the Na intercalation takes place between the layers and the mesopores. Hence, in the presence of mesopores in the carbonaceous materials, Na^+ could smoothly commute in and out of the carbon lattice during the fast charge and discharge process.

Figure 6 indicates galvanostatic charge/ discharge curves of SS with a 0.1 C rate in the voltage range of 0.01 to 3 V. The initial charge capacity has been found as 321.36, 334.85, and 347.39 mAh g^{-1}. This maximum capacity is attributed to the action of chemical activating agents in enhancing the electrochemical performance of the anode material. The SS material sustains a charge capacity of 265.6, 283.84, and 298.6 at the 100th cycle, with coulombic efficiency of 97.6, 98.9, and 99.2 %. Moreover, an average coulombic efficiency of 97, 99, and 99.5% was perceived for K-SS, Na-SS, and Zn-SS samples. The coulombic efficiency of Zn-SS seems to be higher that is owing to the less oxygenated groups present in the material. The K-SS, Na-SS, and Zn-SS samples exhibit capacity retention of 82.6, 84.76, and 85.95% respectively. This high-capacity retention is due to the thermodynamic stability of the as-prepared materials. Fig. 7(c) delineates the rate capability of K-SS, Na-SS, and Zn-SS at various current rates, which respectively exhibit charge capacities of 321.36, 302.8, 276.5, 251.5, 225.8, and 308.36 mAh g^{-1}, 334.85, 310.64, 291.7, 275.9, 248.8, 319.5 mAh g^{-1} and 347.39, 320.85, 299.8, 283.4, 254.62, 336.74 mAh g^{-1} at 0.1, 0.2, 0.5, 1, 2, and then 0.1 C. It was noted that the C rate was reduced from a high 2C rate to 0.1 C rate, and the charge capacities of 308.36, 319.5, and 336.74 mAh g^{-1}, were yet sustained with retention of 95.9, 96.29, and

Table 2
Comparison of various hard carbon as an anode for Sodium-ion batteries.

Carbon precursors	Capacity (mAh g^{-1})	Current density	References
Hard carbon derived from waste tea biomass	282.4	0.1 C	[34]
Hard carbon from sucrose/ PF precursors HCM 1000, HCM 1400, HCM 1600	319, 296, 238.5	0.1 C	[35]
Hard carbon derived from corn straw piths HC 1200, 1400, 1600	290, 310, 191	0.1 C	[36]
Hard carbon derived from walnut shell NDC (Nutshell Derived carbon)	257	50 mA g^{-1}	[37]
Okara-derived Hard carbon	290	50 mA g^{-1}	[38]
Hard carbon derived from Sea sponge	321.36, 334.85, 347.39	0.1 C	This work

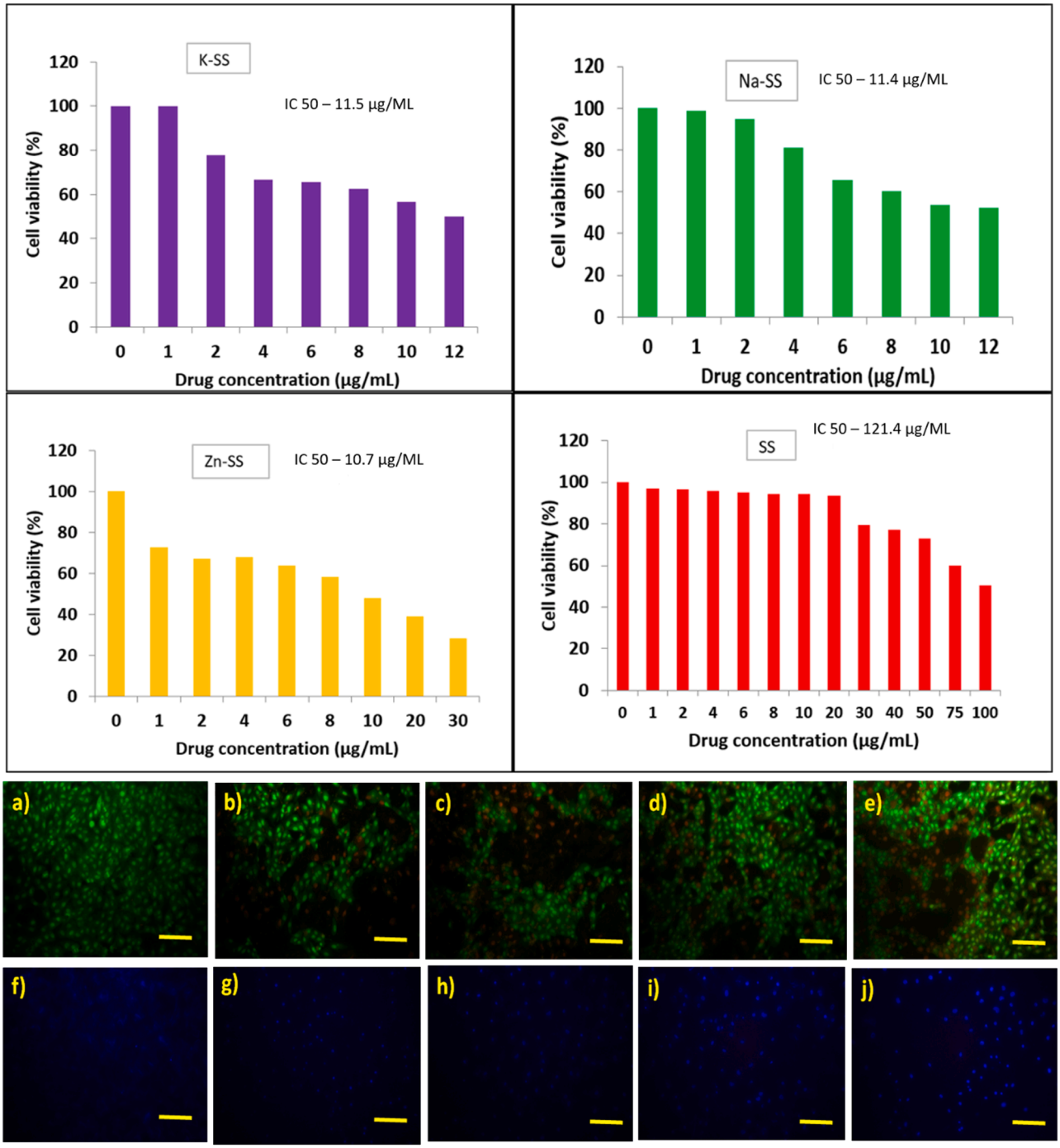

Fig. 8. Cell viability bar diagram and Fluorescence based staining to reveal the induction of apoptosis via dual staining (a–e) and nuclear (f–j) staining by compounds such as SS, K-SS, Na-SS, Zn-SS. (a & f) Control (untreated); (b-g) SS (IC_{50} – 121.4); (c-h)) K-SS (IC_{50} – 11.5); (d-i) Na-SS (IC_{50} – 11.4); (e-j) Zn-SS (IC_{50} – 10.7). Scale bar: 120 µm.

97% for K-SS, Na-SS, and Zn-SS samples respectively. However, it implies that the capacity is higher for Zn-SS for the mesopore structure as a large number of active sodium ions intercalate and deintercalated without any hitch in the electrode material. Besides this, the hard carbon material with mesopore structure is remarkably superintended meant for the maneuverability of alkali ions. As per the earlier reports as itemized in Table 2, the present work illuminates the synthesis of HC anode material by pyrolysis technique and discloses the superior electrochemical performance of sodium-ion batteries.

Figure 7(b) shows the electrochemical impedance spectroscopy (EIS) of the K-SS, Na-SS, and Zn-SS samples. The EIS spectra determine the impedance difference of the system escorted with small amplitude sine wave potential. From Fig. 7(b), all EIS spectra contain a curve in the high-frequency region and a slash in the low-frequency region depicting the impedance information of ion transfer and diffusion process respectively. For the Zn-SS sample, the radius of curvature of the curve decreases when compared to K-SS, and Na-SS. In contemplation of better analysis, the equivalent circuit is espoused to pertinent the impedance spectrum data. Here, R_s is the internal ohmic resistance, R_{ct} is the charge transfer resistance, W_R represents the Warburg resistance and CPE represents the constant phase element. The value of R_{CT} for the K–SS, Na–SS, and Zn–SS cells are 116.02, 110.3, and 97.96 Ω respectively,

which implies that the sodium ions migrate straightforwardly during the cycling process. The decrease in the diameter of the Zn–SS sample is primarily ascribable to the limited formation of the SEI layer. This leads to better cyclability and durability of the anode material. The EIS calculated parameters were shown in table S1. The diffusion coefficient of Na (D_{Na^+}) has been calculated for K-SS, Na-SS and Zn-SS using the formula [33]:

$$D_{Na^+} = \frac{R^2T^2}{2A^2n^4F^4C^2\sigma^2} \quad (3)$$

where R - Gas constant, T - Temperature, A - Area of the electrode, n - Number of electrons migrated, F - Faraday's constant, C - Concentration of Na^+ ions, σ - Coefficient of Warburg impedance. The diffusion coefficient of K-SS, Na-SS and Zn-SS are 3.645×10^{-14}, 6.517×10^{-14}, and 1.15×10^{-15} cm^2/s, respectively.

In the present study, compounds (such as SS, K-SS, Na-SS, and Zn-SS) induced dose-dependent cell death in MDA-MB-231 breast cancer cells (Fig. 8). Table S2 shows the half-maximal inhibitory concentration (IC_{50}) of the compounds. Further, it is reported that activated SS delivered more remarkable results than raw SS. Furthermore, the activated compounds used in the study were found to be biocompatible with normal human embryonic cells (HEK-293) (Table. S2). To study the induction of apoptosis, fluorescence-based probes were used to investigate the induction of apoptosis. Initially, dual staining was performed to distinguish between live (green emission) and dead (red emission) cells subsequent to compound treatment. As anticipated, the compounds induced cell death characterized by red emission with apoptotic morphology (cell blebbing). Hoechst 33,444 staining reveals that the compounds used in the study detect the damaged nuclei, resulting in blue emission. However, control cells were found to have intact nuclear membranes which lack blue emission. Based on the results, it is confirmed that processed samples can be used as an anticancer agent in for biomedical applications.

4. Conclusions

K-SS, Na-SS, and Zn-SS hard carbon materials were successfully synthesized and the influence of the activating agents resulted in better electrochemical performance. The nature of the carbonaceous material was evidenced by XRD and Raman analyses. The existence of mesoporous nature was ascertained through BET analysis. SEM and TEM analyses authorize the porous morphology of K-SS, Na-SS, and Zn-SS, which is held responsible for the intercalation/deintercalation process of Na ions. K-SS, Na-SS, and Zn-SS significantly served as anode material for the SIBs ensuing in capacities of 321.36, 334.85, and 347.39 mAh g^{-1}. The compounds (including SS, K-SS, Na-SS, and Zn-SS) were shown to be biocompatible to normal cells (HEK-293), while also exhibiting significant anti-cancer potential against human breast cancer (MDA-MB-231) cells. Furthermore, the fluorescence microscopic investigation showed that apoptosis was induced due to cell and nuclear membrane damage. Hence, this study conceded that the synthesized K-SS, Na-SS, and Zn-SS disclosed an excellent performance in energy storage and in biomedical applications.

Declaration of Competing Interest

The authors declare that they have no known competing financial interests or personal relationships that could have appeared to influence the work reported in this paper.

Acknowledgments

All the authors from Alagappa University acknowledge the financial support by the Ministry of Human Resource Development RUSA- Phase 2.0 grant sanctioned vide Lt. no. F-24-51/2014U Policy (TNMulti Gen), Dept. of Education, Govt. of India. Also, one of the authors Wei-Ren Liu gratefully acknowledged to National Science of Technology Council (NSTC) project grant No. NSTC 112-2218-E-007-023, 111-2622-E-033-007, 111-2923-E-006-009, 111-2221-E-033-004-MY3 and 112-2218-E-007-023.

Supplementary materials

Supplementary material associated with this article can be found, in the online version, at doi:10.1016/j.jtice.2023.105083.

References

[1] Cheng H, Shapter JG, Li Y, Gao G. Recent progress of advanced anode materials of lithium-ion batteries. J Energy Chem 2021;57:451–68.
[2] Roberts S, Kendrick E. The re-emergence of sodium ion batteries: testing, processing, and manufacturability. Nanotechnol Nano Technol. Sci Appl 2018;11:23–33.
[3] Li Z, Jian Z, Wang X, Rodríguez-Pérez IA, Bommier C, Ji X. Hard carbon anodes of sodium-ion batteries: undervalued rate capability. Chem Commun 2017;53:2610.
[4] She ZW, Sun J, Sun Y, Cui Y. A highly reversible room-temperature sodium metal anode. ACS Cent. Sci. 2015;1:449–55.
[5] Lu Y, Zhao Q, Zhang N, Lei K, Li F, Chen J. Design strategies toward enhancing the performance of organic electrode materials in metal-ion batteries. Adv Funct Mater 2015;26:911–8.
[6] Zhu X, Jiang X, Liu X, Xiao L, Cao Y. A green route to synthesize low-cost and high-performance hard carbon as promising sodium-ion battery anodes from sorghum stalk waste. Green Energy Environ 2017;2(3):310–5.
[7] Wang L, Wang C, Zhang N, Li F, F Cheng F, Chen J. High-performance lithium metal negative electrode with a soft and flowable polymer coating. ACS Energy Lett 2016;2:256–62.
[8] Li M, Carter R, Cohn AP, Pint CL. Interconnected foams of helical carbon nanofibers grown with ultrahigh yield for high-capacity sodium ion battery anodes. Carbon 2016;107:109–15.
[9] Cohn AP, Share K, Carter R, Oakes L, Pint CL. Ultrafast solvent-assisted sodium ion intercalation into highly crystalline few-layered graphene. Nano Lett 2016;16:543–8.
[10] Zhang SW, Lv W, Luo C, You CH, Zhang J, Pan ZZ, Kang FY, Yang QH. Commercial carbon molecular sieves as a high-performance anode for sodium-ion batteries. Energy Storage Mater 2016;3:18–23.
[11] Irisarri E, Ponrouch A, Palacin MR. Hard carbon negative electrode materials for sodium-ion batteries. J Electrochem Soc 2015;162(14):A2476.
[12] Lotfabad EM, Ding J, Cui K, Kohandehghan A, Kalisvaart WP, Hazelton M, Mitlin D. High density sodium and lithium-ion battery anodes from banana peels. ACS Nano 2014;8:7115–29.
[13] Meenatchi T, Subadevi R, Sivakumar M. Hard carbon reprising porous morphology derived from coconut sheath for sodium-ion battery. Energies 2022;15:8086.
[14] Hong KL, Qie L, Zeng R, Yi ZQ, Zhang W, Wang D, Yin W, Wu C, Fan QJ, Zhang WX, Huang YH. Biomass derived hard carbon used as a high-performance anode material for sodium ion batteries. J Mater Chem A 2014;2:12733–8.
[15] Meenatchi T, Priyanka V, Subadevi R, Liu WR, Huang CH, Sivakumar M. Probe on hard carbon electrode derived from orange peel for energy storage applications. Carbon Lett 2021:1–7.
[16] Hou J, Cao C, Idrees F, Ma X. Hierarchical porous nitrogen-doped carbon nanosheets derived from silk for ultrahigh capacity battery anodes and supercapacitors. ACS Nano 2015;9:2556–64.
[17] Li Y, Xu S, Wu X, Yu J, Wang Y, Hu YS, Li H, Chen L, Huang X. Amorphous monodispersed hard carbon micro spherules derived from biomass as a high-performance negative electrode material for sodium-ion batteries. J Mater Chem A 2015;3:71–7.
[18] Ahmadpour A, Do DD. The preparation of active carbons from coal by chemical and physical activation. Carbon 1996;34:471.
[19] Subramanian V, Luo C, Stephan AM, Nahm KS, Thomas S, Wei B. Supercapacitors from activated carbon derived from banana fibers. J Phys Chem C 2007;111:7527–31.
[20] Culwick T, Phillips J, Goodwin C, Rayfield EJ, Hendry KR. Sponge density and distribution constrained by fluid forcing in the deep sea. Front Mar Sci 2020;7:1–12.
[21] Miller RJ, Hocevar J, Stone RP, Fedorov DV. Structure-forming corals and sponges and their use as fish habitat in bering sea submarine canyons. PLoS One 2012;7:e33885.
[22] Anjum K, Abbas SQ, Ali Shah SA, Akhter N, Batool S, Ul Hassan SS. Marine sponges as a drug treasure. Biomol Ther 2016;24:347–62.
[23] Amina M, Al Mussayeib NM. Biological and medicinal importance of sponge. Biol Resour Water 2018:1–13.
[24] Mosmann T. Rapid colorimetric assay for cellular growth and survival: application to proliferation and cytotoxicity assays. J Immunol Methods 1983;65(1-2):55–63.
[25] Kumar P, Senthamilselvi S, Govindaraju M, Sankar R. Unraveling the caspase-mediated mechanism for phloroglucinol-encapsulated starch biopolymer against the breast cancer cell line MDA-MB-231. RSC Adv 2014;4(86):46157–63.
[26] Simoes dos Reiss G, Subramaniyam CM, Angelica DC, Larsson SH, Thyrel M, Lassi U, Garcia-Alvarado F. Facile synthesis of sustainable activated biochars with

different pore structures as efficient additive carbon free anodes for Lithium and sodium-ion batteries. ACS Omega 2022;7:42570–81.
[27] Sandhya RM, Kamaraj M, Ramaprabhu S. Green approach for synthesizing three different carbon microstructures from a single biowaste bombax malabaricum for fully biocompatible flexible supercapacitors and their performance in various electrolytes. ACS Omega 2019;4:6399–410.
[28] Wang N, Liu Q, Boya Sun JG, Yu B, Zhang W, Zhang D. N-doped catalytic graphitized hard carbon for high-performance lithium/sodium-ion batteries. Sci Rep 2018;8:9934.
[29] Huang Y, Wang Y, Bai P, Xu Y. Storage mechanism of alkali metal ions in the hard carbon anode: an electrochemical viewpoint. ACS Appl Mater Interfaces 2021:1–9.
[30] Wang N, Wang Y, Xu X, Liau T, Du Y, Bai Z, Dou S. Defect sites riched porous carbon with pseudocapacitive behavior as an ultrafast and long-term cycling anode for sodium-ion batteries. ACS Appl. Mater. Interfaces 2018:1–27.
[31] Kruk M, Jaroniec M. Gas adsorption characterization of ordered organic-inorganic nanocomposite materials. Chem Mater 2001;13:3169–83.
[32] Poddar P, Asad MA, Islam MS, Sultana S, Nur HP, Chowdhury AS. Mechanical and morphological study of arecanut leaf sheath (ALS), coconut leaf sheath (CLS) and coconut stem fiber (CSF). Adv Mater Sci 2016;1:1–4.
[33] Savithiri G, Priyanka V, Subadevi R, Das BK, Sivakumar M. Enhanced enactment of graphene amalgamated sodium cobalt phosphate composite electrode material in sodium-ion battery. J Taiwan Inst Chem Eng 2021;126:197–204.
[34] Pei L, Cao H, Yang L, Liu P, Zhao M, Xu B, Guo J. Hard carbon derived from waste tea biomass as high-performance anode material for sodium ion batteries. Ionics 2020;26:5535–42.
[35] Zhang H, Ming H, Zhang W, Cao G, Yang Y. Coupled carbonization strategy towards advanced hard carbon for high energy sodium ion battery. ACS Appl Mater Interfaces 2017;9:23766–74.
[36] Zhu Y-E, Gu H, Chen Y-N, Yang D, Wei J, Zhou Z. Hard carbon derived from corn straw piths as anode materials for sodium ion batteries. Ionics 2018;24:1075–81.
[37] SWahid M, Gawli Y, Puthusseri D, Kumar A, Shelke MV, Ogale S. Nutty carbon: morphology replicating hard carbon from walnut shell for Na ion battery anode. ACS Omega 2017;2(7):3601–9.
[38] Yang T, Qian T, Wang M, Shen X, Xu N, Sun Z, Yan C. A sustainable route from biomass byproduct okara to high content nitrogen-doped carbon sheets for efficient sodium-ion batteries. Adv Mater 2016;28:539–45.